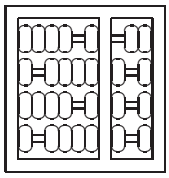

INSTITUTO DE COMPUTAÇÃO
UNIVERSIDADE ESTADUAL DE CAMPINAS

Fast, Accurate and Precise Mid-sagittal Plane Location in 3D MR Images of the Brain

F.P.G. Bergo *A.X. Falcão* *C.L. Yasuda*
G.C.S. Ruppert

Technical Report - IC-08-024 - Relatório Técnico

September - 2008 - Setembro

Fast, Accurate and Precise Mid-sagittal Plane Location in 3D MR Images of the Brain

Felipe P.G. Bergo[1], Alexandre X. Falcão[1],
Clarissa L. Yasuda[2] and Guilherme C.S. Ruppert[1]

[1] LIV – Institute of Computing – University of Campinas (UNICAMP)
CP 6176, 13083-970, Campinas, SP, Brazil.
[2] Dept. of Neurology – Faculty of Medical Sciences – University of Campinas (UNICAMP)
CP 6111. 13083-970, Campinas, SP, Brazil.

Abstract

Extraction of the mid-sagittal plane (MSP) is a key step for brain image registration and asymmetry analysis. We present a fast MSP extraction method for 3D MR images, based on automatic segmentation of the brain and on heuristic maximization of the cerebro-spinal fluid within the MSP. The method is robust to severe anatomical asymmetries between the hemispheres, caused by surgical procedures and lesions. The method is also accurate with respect to MSP delineations done by a specialist. The method was evaluated on 64 MR images (36 pathological, 20 healthy, 8 synthetic), and it found a precise and accurate approximation of the MSP in all of them with a mean time of 60.0 seconds per image, mean angular variation within a same image (precision) of 1.26º and mean angular difference from specialist delineations (accuracy) of 1.64º.

1 Introduction

The human brain is not perfectly symmetric [10, 7, 12]. However, for the purpose of analysis, it is paramount to define and distinguish a *standard of asymmetry*, considered as normal for any given measurement, from abnormal asymmetry, which may be related to neurological diseases, cerebral malformations, surgical procedures or trauma. Several works sustain this claim. For example, accentuated asymmetries between left and right hippocampi have been found in patients with Schizophrenia [32, 8, 26, 21, 14, 2], Epilepsy [15, 33] and Alzheimer Disease [9, 20].

The brain has two hemispheres, and the structures of one side should have their counterpart in the other side with similar shapes and approximate locations [10]. The hemispheres have their boundaries limited by the longitudinal (median) fissure, being the corpus callosum their only interconnection.

The ideal separation surface between the hemisferes is not perfectly planar, but the mid-sagittal plane (MSP) can be used as a reference for asymmetry analysis, without significant loss in the relative comparison between normal and abnormal subjects. The MSP location

is also important for image registration. Some works have used this operation as a first step for intra-subject registration, as it reduces the number of degrees of freedom [1, 18], and to bring different images into a same coordinate system [19], such as in the Talairach [28] model.

The longitudinal fissure forms a gap between the hemispheres filled with cerebro-spinal fluid (CSF). Given that there is no exact definition of the MSP, we define it as a large intersection between a plane and an *envelope* of the brain (a binary volume whose surface approximates the convex hull of the brain) that maximizes the amount of CSF. This definition leads to an automatic, precise, accurate and efficient algorithm for MSP extraction. We have evaluated the precision of the method with respect to random tilts applied to normal and abnormal images. Its accuracy evaluation has also been included, with respect to manual delineations done by a specialist, extending a previous version of this work [4].

The paper is organized as follows. In Section 2, we review existing works on automatic location of the mid-sagittal plane. In section 3, we present the proposed method. In section 4, we show experimental results and validation with simulated and real MR-T1 images. Section 5 states our conclusions.

2 Related works

MSP extraction methods can be divided in two groups: (i) methods that define the MSP as a plane that maximizes a symmetry measure, extracted from both sides of the image [17, 22, 27, 1, 25, 19, 24, 30, 29], and (ii) methods that detect the longitudinal fissure to estimate the location of the MSP [5, 13, 16, 31]. Table 1 summarizes these works, and extensive reviews can be found in [16], [31], [24] and [19].

Methods in the first group address the problem by exploiting the hough symmetry of the brain. Basically, they consist in defining a symmetry measure and searching for the plane that maximizes this score. Methods in the second group find the MSP by detecting the longitudinal fissure. Even though the longitudinal fissure is not visible in some modalities, such as PET and SPECT, it clearly appears in MR images. Particularly, we prefer these methods because patients may have very asymmetric brains and we believe this would affect the symmetry measure and, consequently, the MSP detection.

The aforementioned approaches based on longitudinal fissure detection present some limitations that we are circumventing in the proposed method. In [13], the MSP is found by using snakes and orthogonal regression for a set of points manually placed on each slice along the longitudinal fissure, thus requiring human intervention. Other method [5] uses the Hough Transform to automatically detect straight lines on each slice [5], but it does not perform well on pathological images. The method in [16] assumes local symmetry near the plane, which is not verified in many cases (see Figs. 2, 5 and 8). Volkau et al. [31] propose a method based on the Kullback and Leibler's measure for intensity histograms in consecutive candidate planes (image slices). The method presents excellent results under a few limitations related to rotation, search region of the plane, and pathological images.

Table 1: Summary of existing MSP methods

Method	**Features**	**Measure**
(Brummer, 1991) [5]	Fissure, 2D; MR	Edge Hough Transform
(Guillemaud, 1996) [13]	Fissure, 2D; MR	Active contours
(Hu, 2003) [16]	Fissure, 2D; MR, CT	Local symmetry of fissure
(Volkau, 2006) [31]	Fissure, 3D; MR, CT	Kullback-Leibler's measure
(Junck, 1990) [17]	Symmetry, 2D; PET, SPECT	Intensity cross correlation
(Miroshima,1992) [22]	Symmetry, 3D; PET	Stochastic sign change
(Ardekani, 1997) [1]	Symmetry, 3D; MR, PET	Intensity cross correlation
(Sun, 1997) [27]	Symmetry, 3D; MR, CT	Extended Gaussian image
(Smith, 1999) [25]	Symmetry, 3D; MR, CT, PET, SPECT	Ratio of intensity profiles
(Liu, 2001) [19]	Symmetry, 2D; MR, CT	Edge cross correlation
(Prima, 2002) [24]	Symmetry, 3D; MR, CT, PET, SPECT	Intensity cross correlation
(Tuzikov, 2003) [30]	Symmetry, 3D; MR, CT, SPECT	Intensity cross correlation
(Teverovskiy, 2006) [29]	Symmetry, 3D; MR	Edge cross correlation

3 Methods

Our method is based on detection of the longitudinal fissure, which is clearly visible in MR images. Unlike some previous works, our approach is fully 3D, automatic, and applicable to images of patients with severe asymmetries.

We assume that the mid-sagittal plane is a plane that contains a maximal area of cerebrospinal fluid (CSF), excluding ventricles and lesions. In MR T1 images, CSF appears as low intensity pixels, so the task is reduced to the search of a sagittal plane that minimizes the mean voxel intensity within a mask that disregards voxels from large CSF structures and voxels outside the brain.

The method is divided in two stages. First, we automatically segment the brain and morphologically remove thick CSF structures from it, obtaining a brain mask. The second stage is the location of the plane itself, searching for a plane that minimizes the mean voxel intensity within its intersection with the brain mask. Our method uses some morphological operations whose structuring elements are defined based on the image resolution. To keep the method description independent of image resolution, we use the notation S_r to denote a spherical structuring element of radius r mm.

3.1 Segmentation Stage

We use the tree pruning approach to segment the brain. Tree pruning [3] is a segmentation method based on the Image Foresting Transform [11], which is a general tool for the design of fast image processing operators based on connectivity. In tree pruning, we interpret the

image as a graph, and compute an optimum path forest from a set of seed voxels inside the object. A gradient-like image with high pixel intensities along object borders must be computed to provide the edge weights of the implicit graph. A combinatorial property of the forest is exploited to prune tree paths at the object's border, limiting the forest to the object being segmented.

To segment the brain (white matter (WM), gray matter (GM) and ventricles), we compute a suitable gradient image, a set of seed voxels inside the brain and apply the tree pruning algorithm. A more detailed description of this procedure is given in [3]. Note that any other brain segmentation method could be used for this purpose.

Gradient computation. MR-T1 images of the brain contain two large clusters: the first with air, bone and CSF (lower intensities), and the second, with higher intensities, consists of GM, WM, skin, fat and muscles. Otsu's optimal threshold [23] can separate these clusters (Figs. 1a and 1b), such that the GM/CSF border becomes part of the border between them. To enhance the GM/CSF border, we multiply each voxel intensity $I(p)$ by a weight $w(p)$ as follows:

$$w(p) = \begin{cases} 0 & I(p) \leq m_1 \\ 2\left(\frac{I(p)-m_1}{m_2-m_1}\right)^2 & m_1 < I(p) \leq \tau \\ 2-2\left(\frac{I(p)-m_2}{m_2-m_1}\right)^2 & \tau < I(p) \leq m_2 \\ 2 & I(p) > m_2 \end{cases} \quad (1)$$

where τ is the Otsu's threshold, and m_1 and m_2 are the mean intensities of each cluster. We compute a 3D gradient at each voxel as the sum of its projections along 26 directions around the voxel, and then use its magnitude for tree pruning (Fig. 1c).

Seed Selection. The brighter cluster contains many voxels outside the brain (Fig. 1b). To obtain a set of seeds inside the brain, we apply a morphological erosion by S_5 on the binary image of the brighter cluster. This operation disconnects the brain from adjacent structures. We then select the largest connected component as the seed set (Fig. 1d).

Morphological Closing. The brain object obtained by tree pruning (Fig. 1e) might not include the entire longitudinal fissure, especially when the fissure is too thick. To ensure its inclusion, we apply a morphological closing by S_{20} to the binary brain image (Fig. 1f).

Thick CSF Structure Removal. The last step of this phase is the removal of thick CSF structures (such as the ventricles, lesions and post-surgery cavities) from the brain object, to avoid the MSP from snapping to a dark structure other than the longitudinal fissure. We achieve this with a sequence of morphological operations: we start from a binary image obtained by thresholding at Otsu's optimal threshold (Fig. 1b). We apply a morphological opening by S_5 to connect the thick ($> 5\ mm$) CSF structures (Fig. 1g), and then dilate the result by S_2 to include a thin ($2\ mm$) wall of the CSF structures (Fig. 1h). This dilation

ensures the reinclusion of the longitudinal fissure, in case it is removed by the opening. The binary intersection of this image with the brain object is then used as brain mask (Fig. 1i) by the next stage of our method. Only voxels within this mask are considered by stage 2. Figs. 2a and 2b show how the computed brain mask excludes the large cavity in a post-surgery image, and figures 2c and 2d show how the mask excludes most of the ventricles in patients with large ventricles.

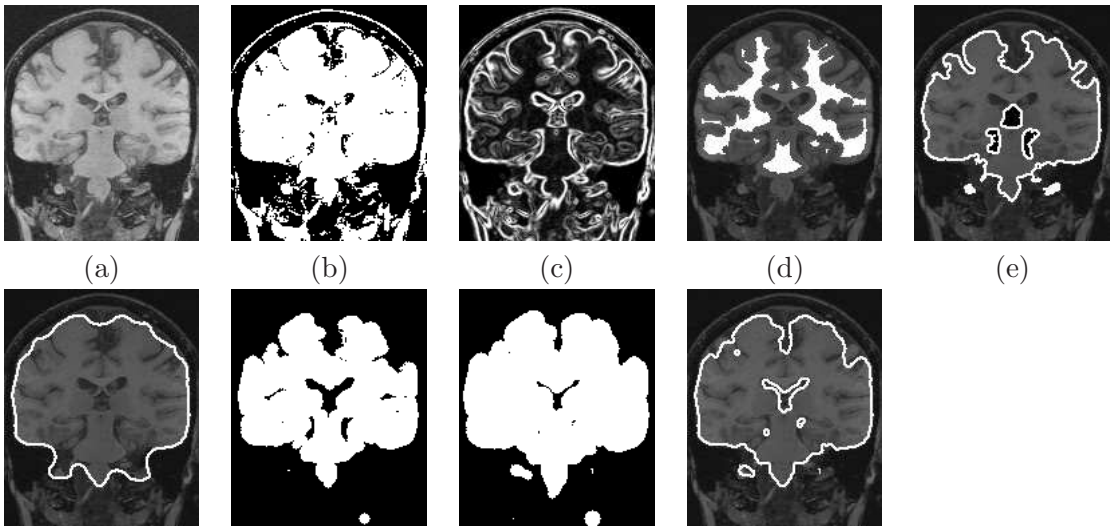

Figure 1: Sample slice of the intermediary steps in stage 1: (a) original coronal MR slice; (b) binary cluster mask obtained by thresholding; (c) gradient-like image used for tree pruning; (d) seed set used for tree pruning (white); (e) border of the brain object obtained by tree pruning (white); (f) border of the brain object after morphological closing; (g) CSF mask after opening; (h) CSF mask after dilation; (h) brain mask (intersection of (f) and (h)).

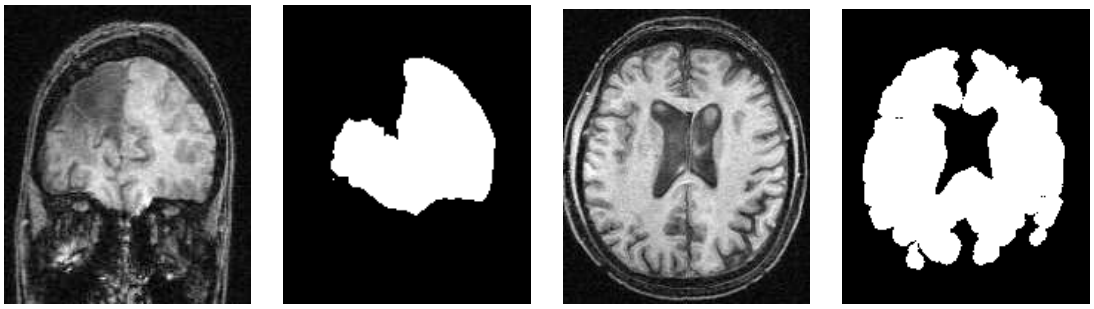

Figure 2: Examples of thick CSF structure removal: (a) coronal MR slice of a patient with post-surgical cavity; (b) brain mask of (a); (c) axial MR slice of a patient with large ventricles; (d) brain mask of (c).

3.2 Plane Location Stage

To obtain the CSF score of a plane, we compute the mean voxel intensity in the intersection between the plane and the brain mask (Figs. 3a and 3b). The lower the score, the more likely the plane is to contain more CSF than white matter and gray matter. The plane with a sufficiently large brain mask intersection and minimal score is the most likely to be the mid-sagittal plane.

To find a starting candidate plane, we compute the score of all sagittal planes in 1 mm intervals (which leads to 140–180 planes in usual MR datasets), and select the plane with minimum score. Planes with intersection area lower than 10 000 mm^2 are not considered to avoid selecting planes tangent to the surface of the brain. Planes with small intersection areas may lead to low scores due to alignment with sulci and also due to partial volume effect between gray matter and CSF (Figs. 3c and 3d).

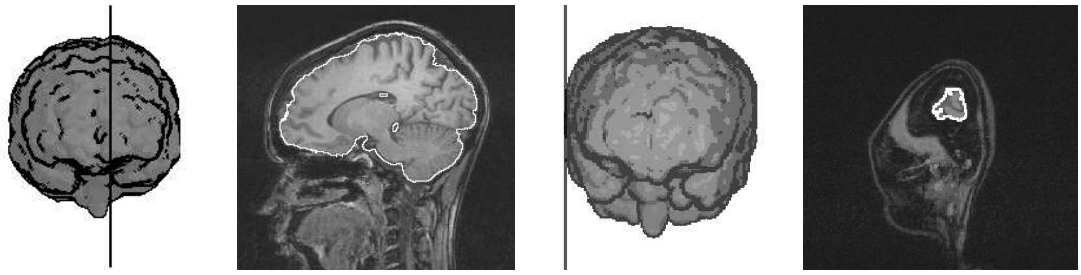

(a) (b) (c) (d)

Figure 3: Plane intersection: (a–b) sample plane, brain mask and their intersection (white outline). (c–d) example of a plane tangent to the brain's surface and its small intersection area with the brain mask (delineated in white), overlaid on the original MR image.

Once the best candidate plane is found, we compute the CSF score for small transformations of the plane by a set of rotations and translations. If none of the transformations lead to a plane with lower CSF score, the current plane is the mid-sagittal plane and the algorithm stops. Otherwise, the transformed plane with lower CSF score is considered the current candidate, and the algorithm is repeated. The algorithm is finite, since each iteration reduces the CSF score, and the CSF score is limited by the voxel intensity domain.

We use a set of 42 candidate transforms at each iteration: translations on both directions of the X, Y and Z axes by 10 mm, 5 mm and 1 mm (18 translations) and rotations on both directions around the X, Y and Z axes by 10^o, 5^o, 1^o and 0.5^o (24 rotations). All rotations are about the central point of the initial candidate plane. Rotations by less than 0.5^o are useless, as this is close to the limit where planes fall over the same voxels for typical MR datasets, as discussed in Section 4.1.

4 Evaluation and Discussion

4.1 Error Measurement

The discretization of $\mathbb{R}^3$ makes planes that differ by small angles to fall over the same voxels. Consider two planes A and B that differ by an angle Θ (Fig. 4). The minimum angle that makes A and B differ by at least 1 voxel at a distance r from the rotation center is given by Equation 2.

$$\Theta = \arctan\left(\frac{1}{r}\right) \tag{2}$$

An MR dataset with 1 mm^3 voxels has a typical maximum dimension of 256 mm. For rotations about the center of the volume, the minimum angle that makes planes A and B differ by at least one voxel within the volume (point p_i in Fig. 4) is approximately $\arctan\left(\frac{1}{128}\right) = 0.45^{\text{o}}$. For most MSP applications, we are only concerned about plane differences within the brain. The largest length within the brain is usually longitudinal, reaching up to 200 mm in adult brains. The minimum angle that makes planes A and B differ by at least one voxel within the brain (point p_b in Fig. 4) is approximately $\arctan\left(\frac{1}{100}\right) = 0.57^{\text{o}}$.

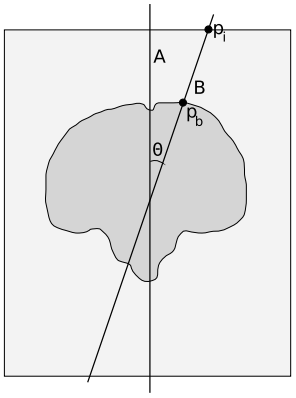

Figure 4: Error measurement in discrete space: points and angles.

Therefore, we can consider errors around 1^{o} excellent and equivalent results.

4.2 Experiments

We evaluated the method on 64 MR datasets divided in 3 groups: A control group with 20 datasets from subjects with no anomalies, a surgery group with 36 datasets from patients with significant structural variations due to brain surgery, and a phantom group with 8 synthetic datasets with varying levels of noise and inomogeneity, taken from the BrainWeb project [6].

All datasets in the control group and most datasets in the surgery group were acquired with a voxel size of $0.98 \times 0.98 \times 1.00$ mm^3. Some images in the surgery group were acquired with a voxel size of $0.98 \times 0.98 \times 1.50$ mm^3. The images in the phantom group were generated

with an isotropic voxel size of 1.00 mm^3. All volumes in the control and surgery groups were interpolated to an isotropic voxel size of 0.98 mm^3 before applying the method.

We performed two sets of experiments: random tilt evaluation (precision) and comparison with expert delineations of the MSPs (accuracy).

4.3 Random Tilt Evaluation

For each of the 64 datasets, we generated 10 variations (tilted datasets) by applying 10 random transforms composed of translations and rotations of up to 12 mm and 12^o in all axes. The MSP location method was applied to the 704 datasets (64 untilted, 640 tilted), and visual inspection showed that the method correctly found acceptable approximations of the MSP in all of them. Fig. 5 shows sample slices of some datasets and the computed MSPs.

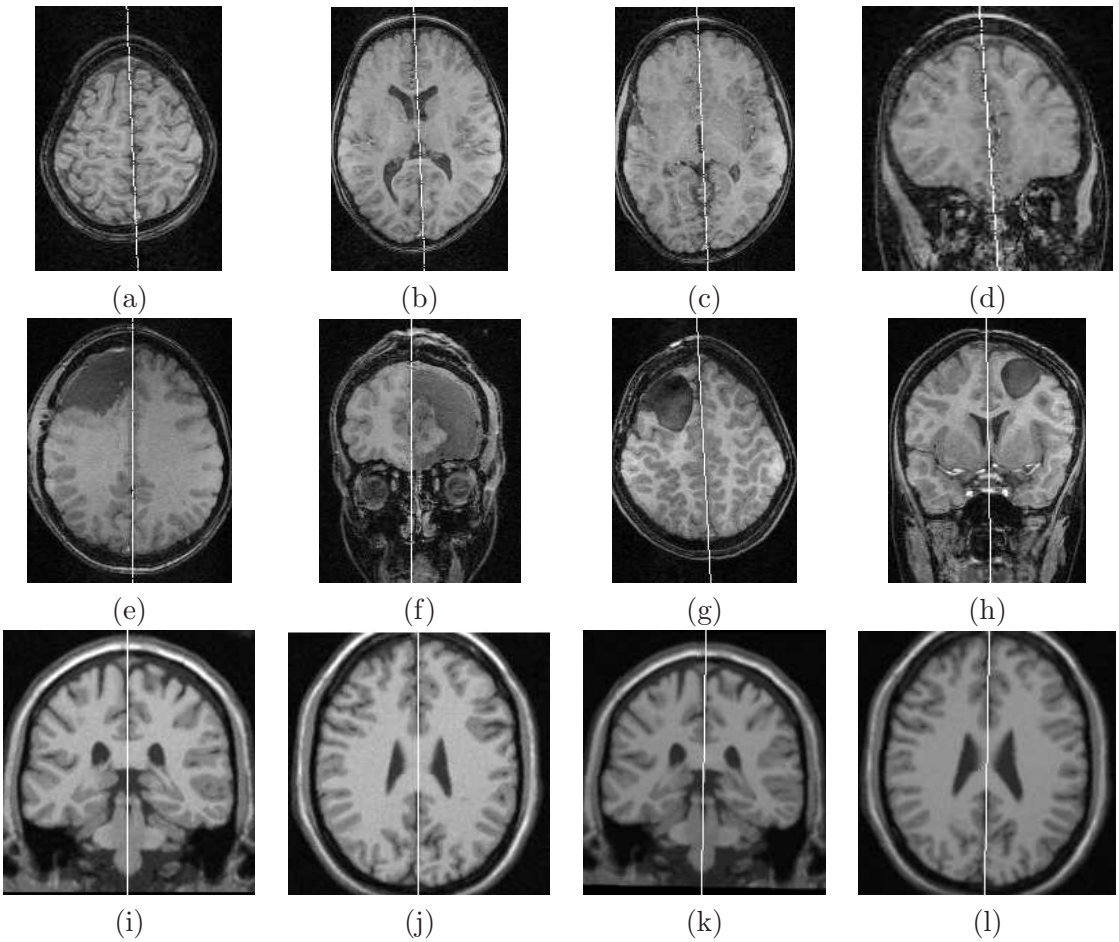

Figure 5: Examples of planes computed by the method: (a–d): sample slices from a control dataset; (e–f) sample slices from a surgery dataset; (g–h) sample slices from another surgery dataset; (i–j): sample slices from a phantom dataset; (k–l): sample slices from a tilted dataset obtained from the one in (i–j).

For each tilted dataset, we applied the inverse transform to the computed mid-sagittal plane to project it on its respective untilted dataset space. Thus, for each untilted dataset we obtained 11 planes which should be similar. We measured the angle between all $\binom{11}{2} = 55$ distinct plane pairs. Table 2 shows the mean and standard deviation (σ) of these angles within each group. The low mean angles (column 3) and low standard deviations (column 4) show that the method is precise and robust with regard to rigid transformations of the input. The similar values obtained for the 3 groups indicate that the method performs equally well on healthy, pathological and synthetic data. The majority (94.9%) of the angles were less than 3°, as shown in the histogram of Fig. 6. Of $64 \times 55 = 3520$ computed angles, only 5 (0.1%) were above 6°. The maximum measured angle was 6.9°. Even in this case (Fig. 7), both planes are acceptable in visual inspection, and the large angle between different two computations of the MSP can be related to the non-planarity of the fissure, which allows different planes to match with similar optimal scores. The lower mean angle in the phantom group (column 3, line 3 of Table 2) can be related to the absence of curved fissures in the synthetic datasets. Fig. 8 shows some examples of non-planar fissures.

Table 2: Angles between computed MSPs in the random tilt evaluation.

Group	**Datasets**	**Angles**	
		Mean	σ
Control	20	1.33°	0.85°
Surgery	36	1.32°	1.03°
Phantom	8	0.85°	0.69°
Overall	64	1.26°	0.95°

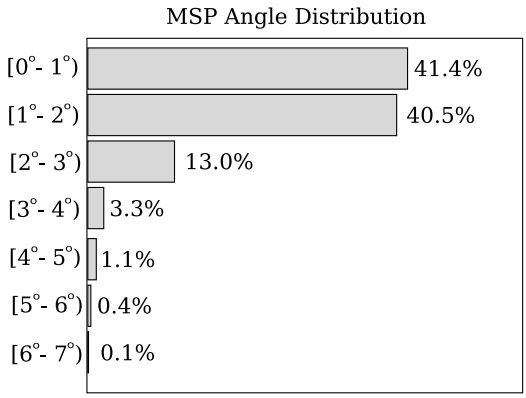

Figure 6: Distribution of the angles between computed mid-sagittal planes in the random tilt experiment.

These experiments were performed on a 2.0 GHz Athlon64 PC running Linux. The method took from 41 to 78 seconds to compute the MSP on each MR dataset (mean: 60.0 seconds). Most of the time was consumed computing the brain mask (stage 1). Stage 1 required from 39 to 69 seconds per dataset (mean: 54.8 seconds), while stage 2 required from 1.4 to 20 seconds (mean: 5.3 seconds). The number of iterations in stage 2 ranged

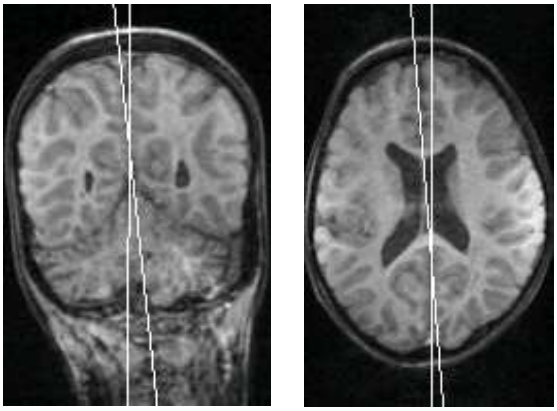

(a) (b)

Figure 7: A coronal slice (a) and an axial slice (b) from the case with maximum angular error (6.9°), with planes in white: The fissure was thick at the top of the head, and curved in the longitudinal direction, allowing the MSP to snap either to the frontal or posterior segments of the fissure, with some degree of freedom.

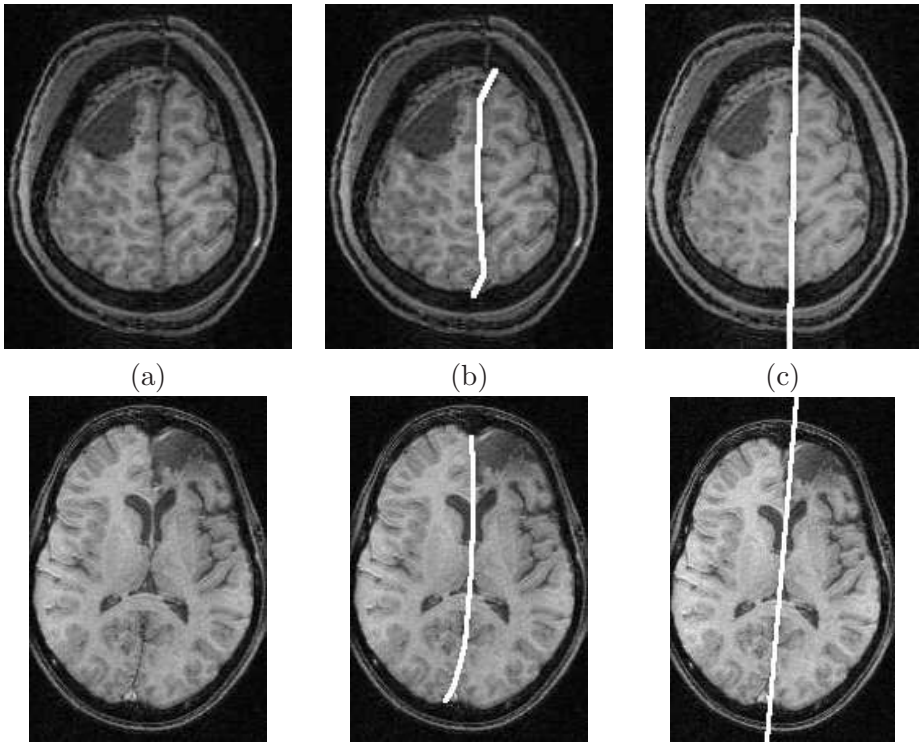

(a) (b) (c)

(d) (e) (f)

Figure 8: Non-planar fissures: (a) irregular fissure, (b) non-planar fissure delineation of (a) by an expert and (c) MSP computed by our method. (d) Curved fissure, (e) non-planar fissure delineation of (d) by an expert and (f) MSP computed by our method.

from 0 to 30 (mean: 7.16 iterations).

4.4 Comparison with Expert Delineations

The MSPs of all 64 images were manually delineated by a specialist (Dr. Yasuda, neurosurgeon). In each image, the specialist selected 10 points over the longitudinal fissure, and the MSP was computed as the minimum squares fit of the points. The fitted plane was displayed interactively as the points were selected, and the specialist was able to inspect the proper location of the plane on any slice (in 3 different orientations), and each of these control points could be dragged with the mouse until the specialist was satisfied with the fitted plane. The specialist took about 2 minutes to delineate the plane on each image. We computed the angles between the manually delineated planes and the MSP located by our method. Table 3 shows the results, and Fig. 9 shows the angle distribution histogram.

Table 3: Angles between computed MSPs and expert delineations.

Group	**Datasets**	**Angles**	
		Mean	σ
Control	20	1.95º	1.23º
Surgery	36	1.62º	1.17º
Phantom	8	0.99º	0.27º
Overall	64	1.64º	1.16º

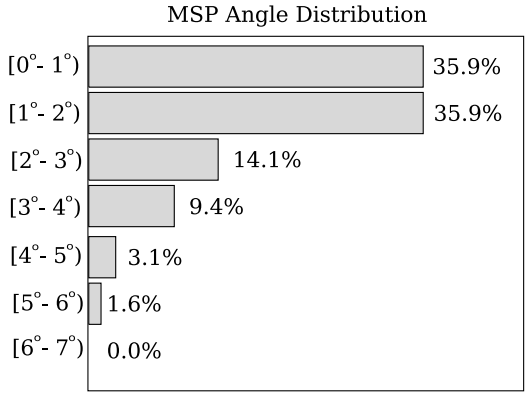

Figure 9: Distribution of the angles between computed mid-sagittal planes and expert delineations.

About 85% of the computed planes matched the specialist's delineation within 3º (Fig. 9). The maximum angular error between a computed MSP and the specialist delineation was 5.7º, which occurred in one of the subjects of the control group. Figs. 10a–e show sample slices from this worst case, and Figs. 10f–h show typical slices from 3 other subjects. The majority of the computed planes closely matched the specialist's delineations. The small angular errors in these cases lead to small offsets in voxel location, considering the discrete image domain.

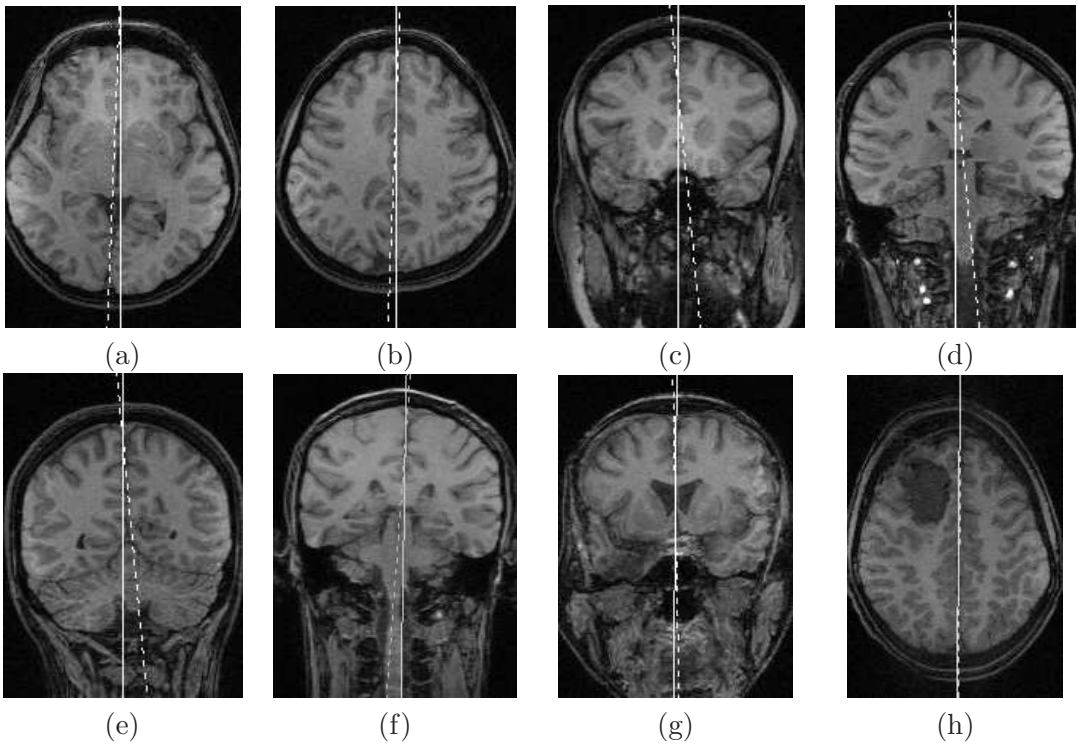

Figure 10: Solid lines represent computed MSPs and dashed lines represent the specialist's delineations. (a)–(e) Sample slices from the single worst case where the computed MSP differed from the specialist's delineation by 5.7º (subject belongs to the control group). (f)–(h): Example slices from 3 distinct images in the surgery group, with angular errors 3.5º (f), 1.6º (g) and 0.3º (h).

5 Conclusions and Future Work

We presented a fast, accurate and precise method for extraction of the mid-sagittal plane from MR images of the brain. It is based on automatic segmentation of the brain and on a heuristic search based on maximization of CSF within the MSP. We evaluated the method on 64 MR datasets, including images from patients with large surgical cavities (Fig. 2a and Figs. 5e–h). The method succeeded on all datasets and performed equally well on healthy and pathological cases. Rotations and translations of the datasets led to mean MSP variations around 1º (high accuracy and repeatability), which is not a significant error considering the discrete space of MR datasets. MSP variations over 3º occurred only in cases where the longitudinal fissure was not planar, and multiple planes fitted different segments of the fissure with similar scores. We compared the MSPs computed by our method with MSP delineations done by a specialist, and over 85% of the computed planes agreed to the specialist's delineation within 3º of difference. The remaining cases were misled by curved fissures and surgical cavities adjacent to the actual fissure. The mean angle variation within a same image (precision) was 1.26º, and the mean angle difference between the computed MSPs and the specialist's delineations (accuracy) was 1.64º. The method required a mean time of 60 seconds to extract the MSP from each MR dataset on a common PC.

Previous fissure-based works were either evaluated on images of healthy patients, on images with small lesions [31], or relied on local symmetry measurements [16]. As future work, we intend to implement some of the previous works and compare their accuracy, precision and performance with our method on the same datasets. Brain mask computation is responsible for most of the computing time. We also plan to evaluate how the computation of the brain mask on lower resolutions affect the accuracy, precision and efficiency of the method.

Acknowledgements

The authors thank CAPES (Proc. 01P-05866/2007), CNPq (Proc. 302617/2007-8), and FAPESP (Procs. 03/13424-1, 05/56578-4, 05/59258-0).

References

[1] B. Ardekani, J. Kershaw, M. Braun, and Iwao Kanno. Automatic detection of the mid-sagittal plane in 3-D brain images. *IEEE Trans. on Medical Imaging*, 16(6):947–952, Dec 1997.

[2] T. R. Barrick, C. E. Mackay, S. Prima, F. Maes, D. Vandermeulen, T. J. Crow, and N. Roberts. Automatic analysis of cerebral asymmetry: na exploratory study of the relationship between brain torque and planum temporale asymmetry. *NeuroImage*, 24(3):678–691, Feb 2005.

[3] F. P. G. Bergo, A. X. Falcão, P. A. V. Miranda, and L. M. Rocha. Automatic image segmentation by tree pruning. *J Math Imaging and Vision*, 29(2–3):141–162, Nov 2007.

[4] F. P. G. Bergo, G. C. S. Ruppert, L. F. Pinto, and A. X. Falcão. Fast and robust mid-sagittal plane location in 3D MR images of the brain. In *Proc. BIOSIGNALS 2008 – Intl. Conf. on Bio-Inspired Syst. and Sig. Proc.*, pages 92–99, Jan 2008.

[5] M. E. Brummer. Hough transform detection of the longitudinal fissure in tomographic head images. *IEEE Trans. on Medical Imaging*, 10(1):66–73, Mar 1991.

[6] D. L. Collins, A. P. Zijdenbos, V. Kollokian, J. G. Sled, N. J. Kabani, C. J. Holmes, and A. C. Evans. Design and construction of a realistic digital brain phantom. *IEEE Trans. on Medical Imaging*, 17(3):463–468, Jun 1998.

[7] T. J. Crow. Schizophrenia as an anomaly of cerebral asymmetry. In K. Maurer, editor, *Imaging of the Brain in Psychiatry and Related Fields*, pages 3–17. Springer, 1993.

[8] J. G. Csernansky, S. Joshi, L. Wang, J. W. Haller, M. Gado, J. P. Miller, U. Grenander, and M. I. Miller. Hippocampal morphometry in schizophrenia by high dimensional brain mapping. *Proceedings of the National Academy os Sciences of the United States of America*, 95(19):11406–11411, Sep 1998.

[9] J. G. Csernansky, L. Wang, S. Joshi, J. P. Miller, M. Gado, D. Kido, D. McKeel, J. C. Morris, and M. I. Miller. Early DAT is distinguished from aging by high-dimensional mapping of the hippocampus. *Neurology*, 55:1636–1643, Dec 2000.

[10] R. J. Davidson and K. Hugdahl. *Brain Asymmetry*. MIT Press/Bradford Books, 1996.

[11] A. X. Falcão, J. Stolfi, and R. A. Lotufo. The image foresting transform: Theory, algorithms and applications. *IEEE Trans. on Pattern Analysis and Machine Intelligence*, 26(1):19–29, Jan 2004.

[12] N. Geschwind and W. Levitsky. Human brain: Left-right asymmetries in temporale speech region. *Science*, 161(3837):186–187, Jul 1968.

[13] R. Guillemaud, P. Marais, A. Zisserman, B. McDonald, T. J. Crow, and M. Brady. A three dimensional mid sagittal plane for brain asymmetry measurement. *Schizophrenia Research*, 18(2–3):183–184, Feb 1996.

[14] J. R. Highley, L. E. DeLisi, N. Roberts, J. A. Webb, M. Relja, K. Razi, and T. J. Crow. Sex-dependent effects of schizophrenia: an MRI study of gyral folding, and cortical and white matter volume. *Psychiatry Research: Neuroimaging*, 124(1):11–23, Sep 2003.

[15] R. E. Hogan, K. E. Mark, I. Choudhuri, L. Wang, S. Joshi, M. I. Miller, and R. D. Bucholz. Magnetic resonance imaging deformation-based segmentation of the hippocampus in patients with mesial temporal sclerosis and temporal lobe epilepsy. *J. Digital Imaging*, 13(2):217–218, May 2000.

[16] Q. Hu and W. L. Nowinski. A rapid algorithm for robust and automatic extraction of the midsagittal plane of the human cerebrum from neuroimages based on local symmetry and outlier removal. *NeuroImage*, 20(4):2153–2165, Dec 2003.

[17] L. Junck, J. G. Moen, G. D. Hutchins, M. B. Brown, and D. E. Kuhl. Correlation methods for the centering, rotation, and alignment of functional brain images. *The Journal of Nuclear Medicine*, 31(7):1220–1226, Jul 1990.

[18] I. Kapouleas, A. Alavi, W. M. Alves, R. E. Gur, and D. W. Weiss. Registration of three dimensional MR and PET images of the human brain without markers. *Radiology*, 181(3):731–739, Dec 1991.

[19] Y. Liu, R. T. Collins, and W. E. Rothfus. Robust midsagittal plane extraction from normal and pathological 3D neuroradiology images. *IEEE Trans. on Medical Imaging*, 20(3):175–192, Mar 2001.

[20] Y. Liu, L. A. Teverovskiy, O. L. Lopez, H. Aizenstein, C. C. Meltzer, and J. T. Becker. Discovery of biomarkers for alzheimer's disease prediction from structural MR images. In *2007 IEEE Intl. Symp. on Biomedical Imaging*, pages 1344–1347. IEEE, April 2007.

[21] C. E. Mackay, T. R. Barrick, N. Roberts, L. E. DeLisi, F. Maes, D. Vandermeulen, and T. J. Crow. Application of a new image analysis technique to study brain asymmetry in schizophrenia. *Psychiatry Research*, 124(1):25–35, Sep 2003.

[22] S. Minoshima, K. L. Berger, K. S. Lee, and M. A. Mintun. An automated method for rotational correction and centering of three-dimensional functional brain images. *The Journal of Nuclear Medicine*, 33(8):1579–1585, 1992.

[23] N. Otsu. A threshold selection method from gray level histograms. *IEEE Trans. Systems, Man and Cybernetics*, 9:62–66, Mar 1979.

[24] S. Prima, S. Ourselin, and N. Ayache. Computation of the mid-sagittal plane in 3D brain images. *IEEE Trans. on Medical Imaging*, 21(2):122–138, Feb 2002.

[25] S. M. Smith and M. Jenkinson. Accurate robust symmetry estimation. In *Proc MICCAI '99*, pages 308–317, London, UK, 1999. Springer-Verlag.

[26] M. Styner and G. Gerig. Hybrid boundary-medial shape description for biologically variable shapes. In *Proc. of IEEE Workshop on Mathematical Methods in Biomedical Imaging Analysis (MMBIA)*, pages 235–242. IEEE, 2000.

[27] C. Sun and J. Sherrah. 3D symmetry detection using the extended Gaussian image. *IEEE Trans. on Pattern Analysis and Machine Intelligence*, 19(2):164–168, Feb 1997.

[28] J. Talairach and P. Tournoux. *Co-Planar Steriotaxic Atlas of the Human Brain*. Thieme Medical Publishers, 1988.

[29] L. Teverovskiy and Y. Liu. Truly 3D midsagittal plane extraction for robust neuroimage registration. In *Proc. of 3rd IEEE Intl. Symp. on Biomedical Imaging*, pages 860–863. IEEE, April 2006.

[30] A. V. Tuzikov, O. Colliot, and I. Bloch. Evaluation of the symmetry plane in 3D MR brain images. *Pattern Recognition Letters*, 24(14):2219–2233, Oct 2003.

[31] I. Volkau, K. N. B. Prakash, A. Ananthasubramaniam, A. Aziz, and W. L. Nowinski. Extraction of the midsagittal plane from morphological neuroimages using the Kullback-Leibler's measure. *Medical Image Analysis*, 10(6):863–874, Dec 2006.

[32] L. Wang, S. C. Joshi, M. I. Miller, and J. G. Csernansky. Statistical analysis of hippocampal asymmetry in schizophrenia. *NeuroImage*, 14(3):531–545, Sep 2001.

[33] W-C. Wu, C-C. Huang, H-W. Chung, M. Liou, C-J. Hsueh, C-S. Lee, M-L. Wu, , and C-Y. Chen. Hippocampal alterations in children with temporal lobe epilepsy with or without a history of febrile convulsions: Evaluations with MR volumetry and proton MR spectroscopy. *AJNR Am J Neuroradiol*, 26(5):1270–1275, May 2005.